THE JOURNAL OF BIOLOGICAL CHEMISTRY VOL. 283, NO. 34, pp. 23093–23103, August 22, 2008

Molecular Determinants of Major Histocompatibility Complex Class I Complex Stability

SHAPING ANTIGENIC FEATURES THROUGH SHORT AND LONG RANGE ELECTROSTATIC INTERACTIONS[*] [S]

Received for publication, December 17, 2007, and in revised form, April 18, 2008 Published, JBC Papers in Press, May 27, 2008, DOI 10.1074/jbc.M710234200

Daniele Narzi[‡1], Kathrin Winkler[§1], Jürgen Saidowsky[§], Rolf Misselwitz[¶], Andreas Ziegler[¶], Rainer A. Böckmann[‡2], and Ulrike Alexiev[§3]

From [‡]Theoretical and Computational Membrane Biology, Center for Bioinformatics, Universität des Saarlandes, P. O. Box 15 11 50, D-66041 Saarbrücken, the [§]Physics Department, Freie Universität Berlin, Arnimallee 14, D-14195 Berlin, and the [¶]Institut für Immungenetik, Charité Universitätsmedizin Berlin, Freie Universität zu Berlin, Thielallee 73, D-14195 Berlin, Germany

A single amino acid exchange between the major histocompatibility complex molecules HLA-B*2705 and HLA-B*2709 (Asp-116/His) is responsible for the emergence of distinct HLA-B27-restricted T cell repertoires in individuals harboring either of these two subtypes and could correlate with their differential association with the autoimmune disease ankylosing spondylitis. By using fluorescence depolarization and pK_a calculations, we investigated to what extent electrostatic interactions contribute to shape antigenic differences between these HLA molecules complexed with viral, self, and non-natural peptide ligands. In addition to the established main anchor of peptides binding to HLA-B27, arginine at position 2 (pArg-2), and the secondary anchors at the peptide termini, at least two further determinants contribute to stable peptide accommodation. 1) The interaction of Asp-116 with arginine at peptide position 5, as found in pLMP2 (RRRWRRLTV; viral) and pVIPR (RRKWRRWHL; self), and with lysine in pΩ, as found in gag (KRWIILGLNK; viral), additionally stabilizes the B*2705 complexes by ~5 and ~27 kJ/mol, respectively, in comparison with B*2709. 2) The protonation state of the key residues Glu-45 and Glu-63 in the B-pocket, which accommodates pArg-2, affects peptide binding strength in a peptide- and subtype-dependent manner. In B*2705/pLMP2, protonation of Glu-45/Glu-63 reduces the interaction energy of pArg-2 by ~24 kJ/mol as compared with B*2705/pVIPR. B*2705/pVIPR is stabilized by a deprotonated Glu-45/Glu-63 pair, evoked by allosteric interactions with pHis-8. The mutual electrostatic interactions of peptide and HLA molecule, including peptide- and subtype-dependent protonation of key residues, modulate complex stability and antigenic features of the respective HLA-B27 subtype.

The presentation of peptides by major histocompatibility complex (MHC)[4] class I molecules at the cell surface and their recognition by cellular ligands like T cell receptors are fundamental for immune responses. The trimeric MHC class I complex consists of a highly polymorphic transmembrane heavy chain (HC) that is noncovalently associated with a light chain, β_2-microglobulin (β_2m) and a peptidic fragment derived from self or non-self proteins. The human MHC class I antigen HLA-B27 is one of the best investigated MHC class I molecules, which is partly due to its strong association with the development of a variety of autoimmune diseases, including ankylosing spondylitis (AS) (1–3). In addition, HLA-B27 is known to present antigenic peptides derived from major infectious agents, such as Epstein-Barr virus, influenza virus, or human immunodeficiency virus (HIV) to cytotoxic T lymphocytes (4–6).

Among the HLA-B27 subtypes, HLA-B*2705 (in short, B*2705) is the most common and exhibits a clear-cut association with AS (7). There is an increasing number of comparative studies between this subtype and HLA-B*2709 (in short, B*2709), which differs from B*2705 only in one amino acid (Asp-116/His) but shows no association to AS (8). A comparison of these very closely related subtypes using functional and structural studies (9–15) as well as various biophysical methods (12, 13, 16–18) may eventually provide clues to the pathogenic role of HLA-B27. Several theories seeking to explain the disease association have been published over the years, most of them regarding the molecule and its peptide binding properties as a key to the pathogenic role of HLA-B27 (7). This holds true for the hypotheses of molecular mimicry between foreign and self-peptides presented by HLA-B27 (14, 15, 17), but also for the

* This work was supported by VolkswagenStiftung Grant I/79 983 (to U. A., R. B., and A. Z.) and in part by Deutsche Forschungsgemeinschaft Grant Sfb 449 TPA5 (to U. A.), Deutsche Forschungsgemeinschaft Grant BIZ 4/1 (to R. A. B.), and European Union Grant EFRE 2000-2006 2ü/2 (to A. Z.). The costs of publication of this article were defrayed in part by the payment of page charges. This article must therefore be hereby marked "*advertisement*" in accordance with 18 U.S.C. Section 1734 solely to indicate this fact.

[S] The on-line version of this article (available at http://www.jbc.org) contains supplemental Tables S1 and S2.

[1] Both authors contributed equally to this work.

[2] To whom correspondence may be addressed. Tel.: 49-681-302-64169; Fax: 49-681-302-64180; E-mail: rainer@bioinformatik.uni-saarland.de.

[3] To whom correspondence should be addressed. Tel.: 49-30-838-55157; Fax: 49-30-83856299; E-mail: alexiev@physik.fu-berlin.de.

[4] The abbreviations used are: MHC, major histocompatibility complex; AS, ankylosing spondylitis; pLMP2, Epstein-Barr virus latent membrane protein 2, residues 236–244 (RRRWRRLTV); pLMP2-T8H, peptide RRRWRRLHV; pVIPR, vasoactive intestinal peptide type 1 receptor, 400–408 (RRKWRRWHL); pVIPR-H8T, peptide RRKWRRWTL; pGR, glucagon receptor 412–420 (RRRWHRWRL); TIS, epidermal growth factor-response factor, 479–487 (RRLPIFSRL); m9, non-natural ligand (GRFAAAIAK); S10R, non-natural ligand (artificial mutant of B*2707 HC 110–119) (RRLLRGHNQY); gag, viral HIV-p24 gag, 263–272 (KRWIILGLNK); flu, influenza nucleoprotein, 383–391 (SRYWAIRTR); pEBNA-3C, Epstein-Barr virus EBNA3C, 258–266 (RRIYDLIEL); KIR3DL1, natural killer Ig-like receptor; LYIA, Lucifer Yellow iodoacetamide; HC, heavy chain; HIV, human immunodeficiency virus; β_2m, β_2-microglobulin.

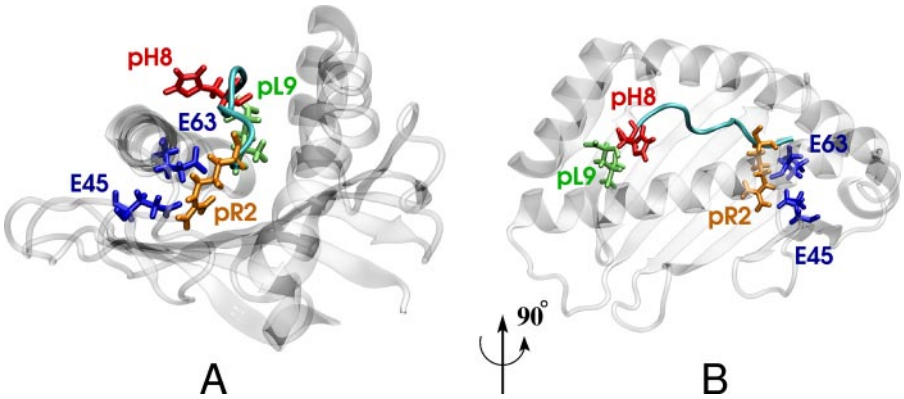

FIGURE 1. **Peptide binding groove of HLA-B27 molecules.** The pVIPR peptide (*cyan*) bound to B*2705 (*gray*) is shown. Glu-45, Glu-63 (*blue*), pArg-2 (*yellow*), pHis-8 (*red*), and pΩ (*green*) are emphasized in *stick representation*. *B* depicts the peptide binding groove as shown in *A* after a 90° rotation about the *vertical axis*.

involvement of misfolded or partially unfolded molecules (19), heavy chain homodimers (20), or liberated β_2m (21). Despite these efforts, the molecular basis of the strong linkage of HLA-B27 with spondyloarthropathies still remains elusive.

Apart from its association to spondyloarthropathies, B*2705 is also connected with the long term nonprogression in chronic HIV infection through the presentation of B*2705-restricted peptides such as gag-(263–272) (KRWIILGLNK) from HIV (22). The recent crystal structure of B*2705 complexed with this peptide demonstrates again the pivotal role of the guanidinium group of arginine at position 2 of the peptide (pArg-2) as the main anchor for the peptide in the B-pocket of the peptide binding groove (23); peptides with an exchange of pArg-2, as observed during HIV infections, fail to be presented by HLA-B27 antigens resulting in immune escape.

Although peptide stability and HLA-B27 selectivity are mainly a consequence of the presence of pArg-2 and its binding within the B-pocket (Fig. 1), every other peptide position may in principle contribute to stable peptide binding (24). The C terminal (pΩ) peptide residue is regarded as a particularly important secondary anchor, which binds within the F-pocket. In B*2705 the acidic Asp-116 at the floor of the peptide binding groove, along with two other F-pocket residues, Asp-74 and Asp-77, plays a key role in the interaction of basic pΩ peptide residues (10, 23). Peptide elution studies showed that the basic amino acids Lys and Arg are strong pΩ anchors for nonameric peptides binding to B*2705. Peptides with pΩArg or pΩLys account for 27% of the natural B*2705 ligands, whereas they are absent (pΩLys) or rare (pΩArg) in the peptide repertoire of B*2709 (24, 25). In addition, Asp-116 has been reported to promote a noncanonical binding mode in two peptides that contain an arginine at position 5 (RRKWRRWHL from a self-protein, pVIPR; and RRRWRRLTV from a viral protein, pLMP2). In this noncanonical binding mode, pArg-5 forms a salt bridge to Asp-116 (11, 14), which presumably adds to the stable accommodation of the respective peptide. In the B*2709 subtype, the exchange of Asp-116 by His does not permit this strong electrostatic interaction.

As the different peptide binding properties of the subtypes also shape the antigenic features for recognition by T cell receptors or other molecules such as inhibitory receptors on natural killer cells (in case of HLA-B27, *e.g.* KIR3DL1) (23), we set out to compare several different peptides (Table 1) in terms of their complex stability and electrostatic interactions between the peptide and the B*2705 and B*2709 subtypes. The results reveal that differences in complex stability as well as in peptide binding affinity between the two very closely related HLA molecules can mainly be explained by changes in the interaction energy between the peptide anchors and the binding groove, although the individual contributions to the peptide binding free energy can differ considerably, even for peptides with high sequence similarity. Furthermore, we find that peptide binding affinities are influenced not only by the expected short range but also by long range interactions between peptide residues and HC amino acids that are crucial in shaping the binding groove.

EXPERIMENTAL PROCEDURES

Protein Preparation—Complexes of the subtypes B*2705 and B*2709 with the peptides m9, pVIPR, TIS, pLMP2, gag, pGR, and the artificial peptide mutants pVIPR-H8T and pLMP2-T8H were prepared as described previously (10, 11, 13–18, 26). The synthetic peptides as well as their fluorescent derivatives labeled with Lucifer Yellow (LY, Molecular Probes) in position C-6 and C-8, respectively, were purchased from Alta Bioscience (Birmingham, UK), Biosynthan (Berlin, Germany), or synthesized in-house. Briefly, heterotrimeric HLA-B27/peptide complexes (HC/β_2m/peptide) were reconstituted from 6 M urea in the presence of the respective peptide. After size exclusion chromatography, the concentrations of highly pure MHC/peptide complexes in 10 mM phosphate buffer, pH 7.5, 150 mM NaCl were adjusted to $A_{426} = 0.0012$ OD using the absorption band of Lucifer Yellow ($\lambda_{max} \approx 430$ nm).

Thermodynamics of Peptide Dissociation—Temperature-induced peptide dissociation from a given MHC/peptide complex was measured by detection of the change in the stationary anisotropy of LY covalently bound to the peptides in the temperature range from 5 to 85 °C (16). An average heating rate of 0.6 °C/min was applied. Lucifer Yellow was excited at $\lambda_{ex} = 428$ nm, and the steady state anisotropy was determined within a time-correlated single photon counting setup (27) by collecting the integral emission intensity for $\lambda \geq 515$ nm parallel $I_{\parallel}$ and perpendicular $I_{\perp}$ with respect to the linearly polarized excitation light. The anisotropy values were calculated according to Equation 1,

$$r(t) = \frac{I_{\parallel}(t) - I_{\perp}(t)}{I_{\parallel}(t) + 2I_{\perp}(t)} \qquad \text{(Eq. 1)}$$

Thermodynamic parameters, such as the enthalpy and entropy changes of the unfolding process as well as transition temperatures (T_m) for peptide dissociation, were obtained by fitting Equation 2 to the steady state anisotropy applying a least square procedure,

$$r(T) = \frac{r_{0b} + s_b T + (r_{0d} + s_d T)\exp\left(\frac{-\Delta H^0_p + T\Delta S^0_p}{RT}\right)}{1 + \exp\left(\frac{-\Delta H^0_p + T\Delta S^0_p}{RT}\right)} \quad \text{(Eq. 2)}$$

with Equation 3

$$T_m = \frac{\Delta H^0_p}{\Delta S^0_p} \quad \text{(Eq. 3)}$$

This equation involves six fitting parameters, respectively; the fluorescence anisotropy of the folded state (native protein), r_{0b}, and of the unfolded or dissociated state, r_{0d}, the temperature dependence of the anisotropy of the peptide-bound (folded) state, S_b, and of the unfolded or dissociated state, S_d, the enthalpy change, ΔH^0_p, and the entropy change, ΔS^0_p, for the two-state dissociation reaction, the thermodynamic quantities being determined at the midpoint of the transition.

HLA-B27 complex unfolding was also followed by the change in the tryptophan fluorescence intensity (16). Comparison of the complex unfolding transition temperatures for HLA complexes with the natural and the LY-labeled peptide (data not shown) indicated that the modification with Lucifer Yellow does not change the thermodynamic properties of the respective complex.

For comparison of the relative complex stability between B*2705 and B*2709 molecules complexed with the same peptide, we calculated the difference in free energy $\Delta\Delta G_{\text{B*2709-B*2705}}$, given by Equation 4,

$$\Delta\Delta G_{\text{B*2709-B*2705}} = \Delta T_{\text{B*2709-B*2705}} \cdot \Delta\bar{S}^0_{\text{B*2709}} \quad \text{(Eq. 4)}$$

$\Delta T_{\text{B*2709-B*2705}}$ is the difference of the peptide dissociation temperatures determined for the complexes B*2705 and B*2709 and $\Delta S^0_{\text{B*2709}}$ is the apparent entropy of the peptide dissociation reaction from B*2709 determined by applying the two-state transition model (Equation 2). According to Becktel and Shellman (28), Equation 4 represents a method for the calculation of free energy differences of biomolecular systems showing only small perturbations, *i.e.* systems that differ only by small modifications, like a single point mutation or the selective binding of a ligand. Because the two HLA-B27 molecules investigated in this study are very closely related and differ only by one amino acid, the conditions for the use of Equation 4 are fulfilled. For the comparison of the relative stability between HLA-B27/pVIPR, HLA-B27/pLMP2, HLA-B27/pVIPR-H8T, and HLA-B27/pLMP2-T8H, respectively, we used the same method, now considering the difference between the sequence-related peptides pVIPR and pLMP2 or their mutants pLMP2-T8H and pVIPR-H8T as a small modification to the system. As the folded protein/peptide complex is characterized by a positive ΔG value, destabilization (stabilization) thus appears as a negative (positive) $\Delta\Delta G$ value (28).

pK_a Analysis—Protein residue pK_a calculations were performed on the crystal structures of the two B*2705 and B*2709 subtypes complexed with several different peptides (pLMP2 (14), pVIPR in both canonical (conformation A) and noncanonical (conformation B) conformations (11), TIS (13), and the model peptide m9 (10)). The pK_a values were also calculated for the B*2709 subtype complexed with the S10R peptide (12) and for the B*2705 subtype complexed with the pGR peptide presented in two different conformations (pGR A and pGR B (15)). The peptides gag-(263–272) (gag) from HIV, EBNA3C-(258–266) (pEBNA-3C) from Epstein-Barr virus, and nucleoprotein 383–391 (flu) from influenza (23) were also included in the study. The resolution of the used crystal structures of the complexes varies from 1.09 to 2.30 Å. The peptides are listed in Table 1. To understand how the presence or absence of a peptide and/or of β_2m in the complex could influence the effective protonation state of the titratable groups, the pK_a calculations were additionally performed on both HLA-B27 subtypes without peptide and with or without β_2m. Peptide mutants were obtained as follows: pHis-8 of pVIPR was mutated with a threonine using the WHAT IF (29) package (experimental version of the function mutate (30)). For the exchange of pThr-8 in pLMP2 with a histidine, a different strategy was adopted; after fit of the peptide backbone atoms of residues 7 to 9, the side chain of pThr-8 in pLMP2 was replaced by the side chain of the pHis-8 in pVIPR B, followed by a short energy minimization of the structure using a steepest descent algorithm (100 steps).

The pK_a calculations were based on the scheme proposed by Nielsen *et al.* (31–33), which combines finite difference solutions to the Poisson-Boltzmann equation with a global optimization of the hydrogen bond network in all protonation states. All radii and charges of the atoms were taken from the OPLS force field (34). The linearized Poisson-Boltzmann equation was solved applying DELPHI II (35), with the parameters used in Ref. 32; a dielectric constant of 80 for water and 8 for the protein interior, a 65 cubed grid, a grid resolution of 3 grid points/Å for the desolvation energy and of 4 grid points/Å for the background interaction energy, a 2.0 Å ion exclusion layer, an ionic strength of 0.144 M, and a surface probe radius of 1.4 Å have been used. As suggested previously by Nielsen and Vriend (31), a locally increased dielectric constant of 16 was applied for partially solvent-exposed amino acids. This increased dielectric constant was taken into account for residues that have an accessible alternative rotamer or a *B*-factor above a specified value B_{crit} (31). To avoid artifacts due to the varying resolution of the crystal structures and therefore also varying average *B*-factors, B_{crit} was adjusted such that the buried titratable residues in the various crystal structures were consistently assigned the interior dielectric constant of 8.

The interaction energy between the anchor amino acid pArg-2 and the B-pocket was estimated from the sum of the van der Waals and the Coulomb interactions (no cut-off applied) between pArg-2 and the HLA-B27 molecule, excluding the interactions with the remainder of the bound peptide. As a rough description of the dielectric screening, a distance-dependent dielectric constant of $\epsilon = 4r$ was applied. The interaction energy was calculated after minimization was carried out with the GROMACS software package version 3.3.1 (36–38) using the all-atom OPLS force field (34) (criterium for minimization, maximum force smaller than 100 kJ mol^{-1} nm^{-1}). The interaction energy was computed for different protonation states of the HC glutamic acids in positions 45 and 63.

For the sequence-similar pVIPR and pLMP2 peptides, additionally the enthalpic part of the binding free energy $\Delta G_{\text{binding}} =$

$\Delta G_{complex} - \Delta G_{free}$ was estimated by the sum of the van der Waals interaction energy ΔG_{vdW} and the Coulomb interaction energy ΔG_{Coul} between the peptide and the HLA-B27 molecule and the difference in solvation free energies between the complex and the free state as shown in Equation 5.

$$\Delta G_{binding} \approx \Delta G_{vdW} + \Delta G_{Coul} + \Delta G_{solvation} - T\Delta S \quad \text{(Eq. 5)}$$

The entropic contribution $T\Delta S$ to the binding free energy is assumed to be equal for the binding of the sequence-similar pVIPR and pLMP2 peptides to a specific HLA-B27 subtype. Equation 5 thus allows a comparison of the binding free energies between these peptides ($\Delta\Delta G_{binding}$).

The solvation free energy $\Delta G_{solvation}$ is approximated as the sum of the electrostatic solvation ($\Delta G_{elec.solv.}$) and nonpolar energy ($\Delta G_{nonpolar}$) contributions (39). The former is computed by numerical solution of the (nonlinear) Poisson-Boltzmann equation using the DELPHI II (35) package, and the latter is approximated to depend linearly on the solvent-accessible surface (39). No cut-off has been applied in the calculation of the Coulomb and van der Waals interaction energies.

The computed total binding free energies ($\Delta G_{binding,0/-}$ and $\Delta G_{binding,-/-}$, compare Fig. 2) had to be corrected for contributions due to de-protonation of a glutamic acid (Glu-45/Glu-63) upon peptide binding to the HLA molecule ($\Delta G_{pKa,HLA}$ and $\Delta G\, G_{pKa,HLA/peptide}$, see Fig. 2). A similar contribution had to be taken into account due to the de-protonation of a lysine in position 3 of the VIPR peptide upon binding to B*2709 (see "Results"). The corrections depend on the pK_a of the amino acid changing its protonation state. This term can easily be evaluated considering the thermodynamic cycle shown in Fig. 2 and is given by Equation 6 (40),

$$\Delta G_{pK} = k_b T \ln(10) \cdot (pK_a - pH_{exp}) \quad \text{(Eq. 6)}$$

pH_{exp} is the experimental pH 7.5. For peptides that, for example, de-protonate Glu-45 upon binding to B*2705, $pK_a = 10.2$ is the pK_a value of Glu-45 in the B*2705 subtype in the absence of a peptide (see Table 4 for pK_a values of the various peptide-bound complexes). Errors for the difference in the binding free energies are estimated to 6 kJ/mol.

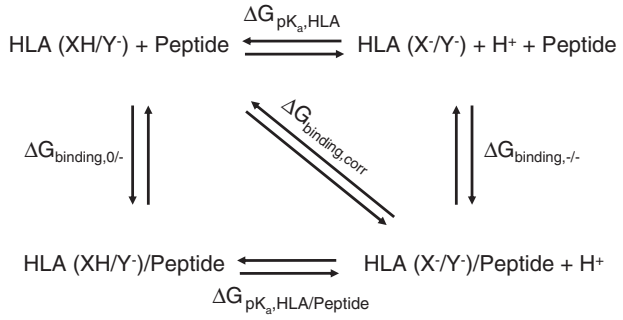

FIGURE 2. **The general thermodynamic cycle used for the calculation of the peptide binding affinity.** $\Delta G_{pK,HLA/Pep}$ ($\Delta G_{pK,HLA}$) is the free energy difference associated with the deprotonation of the Glu-45/Glu-63 residue in the HLA-peptide complex (empty HLA molecule) (see Equation 6). To account for protonation changes of Glu-45/Glu-63 upon peptide binding, a corrected peptide binding affinity was used for the calculation: $\Delta G_{binding,corr} = \Delta G_{binding} + \Delta G_{pK}$. *X/Y* denotes the Glu-45/63 pair.

RESULTS

Choice of Peptides—The HLA-B27/peptide complexes were analyzed with regard to two properties, thermal stability and a possible dependence of the protonation states of HC residues on the bound peptide. We chose 12 peptides for our studies (Table 1). For most of these peptides x-ray data are available either from B*2705 and B*2709 (m9, TIS, pVIPR, and pLMP2), from B*2705 (pGR, pEBNA-3C, flu, and gag), or only from B*2709 (S10R).

Spectroscopic Characterization of the HLA Molecules Complexed with Fluorescently Labeled Nonameric Peptides—Purified soluble B*2705 and B*2709 molecules refolded with the different peptides m9, TIS, pVIPR, pVIPR-H8T, pLMP2, pLMP2-T8H, pGR, and gag, labeled with the fluorescence dye LY at positions p6 or p8 via Cys residues that replace the respective peptide amino acids, were characterized by absorption and fluorescence spectroscopy. As an example, the absorption and emission spectra of the complex B*2705/pLMP2-C6-LY are shown in Fig. 3, *A* and *B*, respectively. The absorption spectrum of the complexes is characterized by a weak absorption band centered at 428 ± 1 nm for m9, TIS (13, 16, 18), and gag (data not shown) and 431 ± 2 nm for pVIPR (16), pLMP2 (Fig. 3*A*), and pGR (data not shown), respectively, which is because of the absorption of the fluorescent label LY attached to the peptide. A strong band at 280 nm represents the transition of LY to higher electronic states and the absorption of tryptophan residues in the HC and β_2m. The emission spectrum (Fig. 3*B*) shows the fluorescence of LY with a maximum at $\lambda_{max} = 533 \pm 2$ nm.

Thermal Stability of HLA-B27/Peptide Complexes—The stabilities of the different HLA-B27/peptide complexes were assessed by investigating their thermal behavior. From temper-

TABLE 1

B*2705 or B*2709 bound peptides investigated in this study

The citation after each abbreviation represents the reference where the crystal structure of the given HLA-B27/peptide complex is published.

Sequence	Origin/peptide	Abbreviation
R**R**LPIFSR**L**	Human self-peptide: epidermal growth factor response factor, residues 479–487	TIS (13)
R**R**KWRRWH**L**	Human self-peptide: vasoactive intestinal peptide type 1 receptor, 400–408	pVIPR (11)
R**R**KWRRWT**L**	Artificial mutant of pVIPR	pVIPR-H8T
R**R**RWHRWR**L**	Human self-peptide: glucagon receptor, 412–420	pGR (15)
R**R**RWRRLT**V**	Viral: Epstein-Barr virus latent membrane protein 2, 236–244	pLMP2 (14)
R**R**RWRRLH**V**	Artificial mutant of pLMP2	pLMP2-T8H
R**R**IYDLIE**L**	Viral: Epstein-Barr virus EBNA3C, 258–266	pEBNA-3C (23)
R**R**IYDLIT**L**	Artificial mutant used for pK_a calculations	pEBNA-3C-E8T
S**R**YWAIRT**R**	Viral: influenza virus nucleoprotein, 383–391	flu (23)
K**R**WIILGLN**K**	Viral: HIV-p24 gag, 263–272	gag (23)
G**R**FAAAIA**K**	Non-natural ligand	m9 (10)
R**R**LLRGHNQ**Y**	Non-natural ligand (artificial mutant of B*2707 HC 110–119)	S10R (12)

ature-induced peptide dissociation experiments, thermodynamic parameters were derived such as the apparent enthalpy, entropy, and transition temperature of the peptide dissociation process. Monitoring the fluorescence polarization or anisotropy of the labeled peptide is especially suited to directly follow the molar fraction of the peptide molecules bound to the complex and the fraction of peptides free in solution (16, 18, 41, 42).

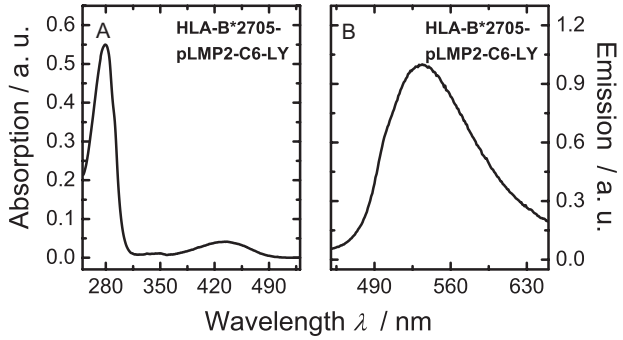

FIGURE 3. **Absorption (*A*) and emission spectra (*B*) of the HLA-B*2705/pLMP2-C6-LY complex.** Lucifer Yellow was excited at λ_{ex} = 428 nm. Conditions are as follows: 0.3 μM HLA-B27/peptide complex dissolved in 10 mM sodium phosphate buffer, 150 mM NaCl, pH 7.5.

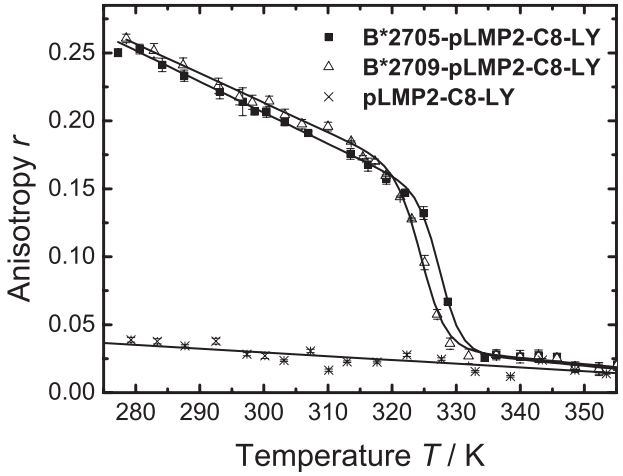

FIGURE 4. **Steady state fluorescence anisotropy of HLA-B*2705/pLMP2-C8-LY (*squares*), B*2709/pLMP2-C8-LY (*triangles*), and the labeled peptide (*crosses*) as a function of temperature.** Each data point represents the mean of five measurements. The S.E. is given. Conditions are as in Fig. 3.

Fig. 4 shows the dissociation of pLMP2-C8-LY from B*2709 and B*2705, respectively, as observed by the change in steady state fluorescence anisotropy of the fluorescent dye. A single two-state transition for peptide dissociation is sufficient to describe the unbinding of pLMP2 from B*2705 and B*2709 with a transition temperature of T_m = 55.0 ± 0.2 °C and T_m = 52.0 ± 0.2 °C, respectively. Table 2 summarizes the transition temperatures for peptide unbinding from B*2705 and B*2709. For m9, gag, pVIPR, and pLMP2, the thermal stability is higher in the complex with B*2705 than with B*2709. In contrast, for TIS and pGR a slightly increased stability in the complex with the subtype B*2709 was observed. The differences in HLA-B27/peptide complex stability were further quantified in terms of free energy differences for peptide unbinding between the two subtypes, $\Delta\Delta G$ (Equation 4, see "Experimental Procedures"), and are explained below (Table 2).

The two peptides pLMP2 and pVIPR (in its conformation B (in short pVIPR B)) (11) display an unusual noncanonical peptide binding mode when refolded with B*2705. This binding mode is mediated by the additional salt bridge between Asp-116 and pArg-5, which is absent in the subtype B*2709 because of the natural Asp-116/His exchange (11, 14). Our results reveal a gain in B*2705/peptide complex stability compared with the respective B*2709/peptide complex of ~4–7 kJ/mol (Table 2), most likely because of this additional salt bridge. This value, however, is much lower than the gain in peptide stabilization observed in connection with an additional salt bridge between the secondary anchor residue pLysΩ (m9 and gag peptide) with Asp-116 in the B*2705/m9 and B*2705/gag complex, respectively, in comparison with the respective B*2709 complexes. Here we observed a stabilization of ~7–27 kJ/mol for the complexes with B*2705 as compared with the complexes with B*2709

TABLE 2

Thermal peptide unbinding parameters as measured by steady state fluorescence depolarization of the LY-labeled peptide

The conditions used are as follows: 10 mM sodium phosphate buffer, pH 7.5, 150 mM NaCl. Negative (positive) values of $\Delta\Delta G_{B*2709\text{-}B*2705}$ denote a destabilization (stabilization) of the B*2709/peptide complex compared with the B*2705/peptide complex.

Peptide	Subtype	T_m	$\Delta T_{B*2709\text{-}B*2705}$	ΔS^0_{B*2709}	$\Delta\Delta G_{B*2709\text{-}B*2705}$
		K	*K*	*J mol^{-1} K^{-1}*	*kJ mol^{-1}*
pVIPR[a]	B*2705	337.5 ± 1.8			
-C6/C8-LY	B*2709	330.2 ± 1.9	−7.3 ± 3.7	939 ± 70	−6.9 ± 4.2
pLMP2[a]	B*2705	326.7 ± 0.25			
-C6/C8-LY	B*2709	323.3 ± 1.95	−3.4 ± 2.2	1236 ± 110	−4.2 ± 3.1
pGR[b]	B*2705	330.5 ± 0.2			
-C6-LY	B*2709	331.7 ± 0.1	+1.2 ± 0.2	1381 ± 30	+1.7 ± 0.3
TIS[a,c]	B*2705	331.4 ± 0.4			
-C6-LY	B*2709	333.3 ± 0.4	+1.9 ± 0.7	1040 ± 330	+2.0 ± 1.4
gag[d]	B*2705	340.9 ± 0.7			
-C6-LY	B*2709	321.6 ± 2.6	−19.3 ± 3.2	1380 ± 5	−26.6 ± 0.3
m9[a,e]	B*2705	339.5 ± 1.1			
-C6/C8-LY	B*2709	320.0 ± 1.0	+19.5 ± 2.1	870 ± 40	−17.0 ± 1.9
pVIPR-H8T-C6-LY[d]	B*2705	333.1 ± 1.1			
pLMP2-T8H-C6-LY[d]	B*2705	324.1 ± 0.7			

[a] Mean values were obtained from the temperature dependence of the anisotropy data with the fluorescent label attached to pC6 and pC8. The S.E. is given. For each peptide at least 10 measurements from two independent sample preparations were averaged. For pVIPR-C8-LY, the peptide dissociation data obtained from the change in fluorescence intensity of LY were included (16).
[b] Average from two independent sample preparations with at least 10 measurements.
[c] Based on the comparison of crystallographic and thermodynamic data, only values obtained with TIS-C6-LY were included (13).
[d] Average from two independent measurements.
[e] Data for m9-C6-LY are from Pöhlmann *et al.* (16).

(Table 2). Additionally, we observe very similar thermal stabilities of B*2705 (T_m = 67–68 °C) when complexed either with m9 or gag and also for B*2709 (T_m = 47–49 °C), which emphasizes the importance of pLysΩ in these peptides.

The peptide TIS displays a canonical binding mode in which the side chain of pLeuΩ interacts via hydrophobic interactions with F-pocket residues (13). In case of pGR, which exhibits high sequence similarity with pLMP2 and pVIPR, the peptide is bound to B*2705 in a double nonstandard conformation in which pHis-5 is not directly connected to Asp-116, in contrast to pArg-5 of the pVIPR and pLMP2 peptides (15). Both peptides (TIS, pGR) exhibit transition temperatures for thermal peptide unbinding in the narrow range between 57 and 60 °C (330 and 333 K), regardless of their binding to B*2705 or B*2709. The B*2709-TIS(pGR) complex is slightly more stable by about 2 kJ/mol with respect to the B*2705/TIS(pGR) complex.

For a better comparison between these five peptides, we plotted the transition temperatures (Table 2) as the difference to a reference T^*_m value of 59 °C in Fig. 5. The reference T^*_m is close to the T_m value of the peptides pGR and TIS, which lack the arginine at peptide position 5. Both the m9 and the pVIPR peptide complexed with B*2705 display an increased T_m in comparison with T^*_m, as expected from the additional salt bridge of Asp-116 to pLysΩ for m9 (10) or to the central pArg-5 for pVIPR (11). In contrast, and despite its salt bridge to Asp-116, B*2705-pLMP2 shows a decrease in T_m as compared with T^*_m.

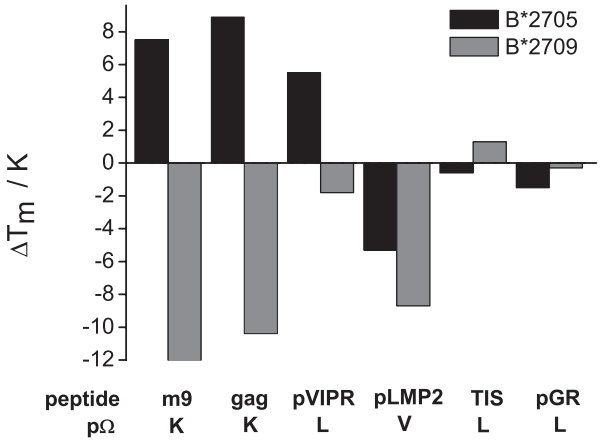

FIGURE 5. **Transition temperatures for peptide dissociation (T_m) from the respective complexes with HLA-B*2705 and HLA-B*2709.** The *histogram* shows the change in T_m (ΔT_m) compared with T^*_m = 59 °C (see text). The T_m values are taken from Table 2.

The destabilization energy $\Delta\Delta G$ between the two structurally and sequence-related peptides pVIPR and pLMP2 calculated from the thermodynamic parameters according to Equation 4 amounts to about −18 kJ/mol in B*2705 and to about −9 kJ/mol in B*2709 (Table 3). Thus, in both subtypes the HLA-B27/peptide complex stability is reduced for HLA-B27/pLMP2 compared with HLA-B27/pVIPR as deduced from the negative value of the free energy difference of peptide unbinding. This effect, however, is less pronounced in the subtype B*2709 (about 50% of the B*2705 value).

Electrostatics of Peptide Binding—To solve the puzzle of the unexpected destabilization of the HLA-B27-pLMP2 complexes, we performed extended electrostatic calculations to analyze the contribution of titratable groups in the peptide binding groove to stable peptide accommodation. All crystal structures of B*2705/peptide and B*2709/peptide complexes that are available from the literature (see Table 1) were included in this study.

In agreement with the overall structural similarity of the crystal structures, only minor changes in the pK_a values of titratable groups were found for the different complexes. However, there were two exceptions as follows: Glu-45 and Glu-63 show peptide-dependent protonation states. These two amino acids are involved in binding of the main anchor pArg-2 within the B-pocket (see Fig. 1). The effective pK_a values of Glu-45 and Glu-63 with the respective protonation states at physiological pH (for every system studied) are reported in Table 4.

Our pK_a calculations reveal the presence of a protonated Glu-45 (p$K_a > 7.5$) in both B*2705 and B*2709 complexed to the viral peptide pLMP2, for all investigated viral peptides (gag, pEBNA-3C, flu) bound to B*2705, and in both subtypes in the peptide-devoid state. Also, pVIPR bound to B*2709 results in a protonated Glu-45. In contrast, Glu-45 is preferably unprotonated (p$K_a < 7.5$) at physiological pH in both subtypes when complexed with TIS and the m9 peptide, in B*2709 with pS10R, and in B*2705 presenting pVIPR and pGR (see protonation states of Glu-45 in Table 4). However, increased pK_a values with respect to the model pK_a of 4.4 were observed for the B*2705 subtype complexed with the self-peptide pVIPR (p$K_a \approx 6$) and the model peptide m9 (7.4). For those peptides with increased pK_a values for Glu-45, the titration curves suggest a shared proton between Glu-45 and Glu-63 at low pH (see Fig. 6, *red* and *blue lines* for pVIPR as an example). Shared protons have been suggested before based on the distances between the Glu-63 OE1 and Glu-45 OE2 atoms in the crystal structure of the B*2705 complexes with pEBNA-3C, flu, and gag peptides as

TABLE 3

Change in free energy of thermal peptide stability for the peptide pLMP2 in comparison with pVIPR when bound to the B*2705/09 subtypes

The HLA complexes were compared at pH 7.5. The transition temperatures for peptide unbinding are given in Table 2. The mean values for ΔT_m and ΔS^0 were obtained from the respective data with the fluorescent label attached to pC6 and pC8. $\Delta\Delta G_{\text{pLMP2-pVIPR}}$ was calculated according to Equation 4. The S.E. is given. The computed differences in the binding free energy $\Delta\Delta G_{\text{pLMP2-pVIPR,calc}}$ were obtained by averaging the free energies for both protonated states (Glu-45 protonated or Glu-63 protonated). For pVIPR, the canonical (conformation A, in short A) and the noncanonical conformation (conformation B, in short B) were considered, and differences in entropy for binding of these sequence-similar peptides to the same HLA subtype were neglected (see supplemental Table S2). The same holds true for the interaction energy (electrostatic and van der Waals) between pArg-2 and the respective subtype $\Delta E_{\text{pArg-2,calc}}$ (see Table 5). Negative (positive) energy differences denote a destabilization (stabilization) of HLA-B27/pLMP2 complex compared to HLA-B27/pVIPR.

Subtype	$\Delta T_{\text{pLMP2-pVIPR}}$	$\Delta S^0_{\text{pLMP2}}$	$\Delta\Delta G_{\text{pLMP2-pVIPR}}$	$\Delta\Delta G_{\text{pLMP2-pVIPR,calc}}$	$\Delta E_{\text{pArg-2,calc}}$
	K	*J mol*$^{-1}$ *K*$^{-1}$	*kJ mol*$^{-1}$	*kJ mol*$^{-1}$	*kJ mol*$^{-1}$
B*2705	−10.8 ± 0.1	1687 ± 160	−18.2 ± 2.2	−20 ± 6 (B) +8 ± 6 (A)	−24 ± 6 (B) −25 ± 6 (A)
B*2709	−6.9 ± 3.4	1236 ± 110	−8.5 ± 4.9	−2 ± 6	+11 ± 6

TABLE 4

pK_a values for all crystal structures of B*2705/09

The pK_a values of Glu-45 and Glu-63 as well as the preferred protonation states at physiological pH) (PS: 0, protonated, –, charged) are given. In those cases where a proton is shared by both Glu-45 and Glu-63 (marked by boldface) the pK_a is calculated from the sum of both titration curves and assigned to the glutamic acid with the larger protonation fraction at physiological pH. pVIPR A and B denote the canonical (p4α) and noncanonical (p6α) peptide conformation (11).

Subtype	Glu-45	PS	Intrinsic pK_a	Glu-63	PS	Intrinsic pK_a
B*2705 pLMP2	**8.8**	0	8.1	**0.0**	–	6.0
B*2709 pLMP2	**8.7**	0	9.0	**0.0**	–	5.8
B*2705 pVIPR A	**6.0**	–	8.0	**0.0**	-	6.0
B*2705 pVIPR B	**6.4**	–	8.0	**0.0**	–	6.0
B*2709 pVIPR	13.1	0	8.3	0.0	–	5.8
B*2705 pVIPR B H8T	9.0	0	8.1	0.0	–	6.0
B*2705 pLMP2 T8H	6.1	–	8.5	0.0	–	7.4
B*2705 TIS	0	–	7.0	0.0	–	5.9
B*2709 TIS	0	–	8.2	0.8	–	6.9
B*2705 m9	7.4	–	8.4	0.0	–	5.1
B*2709 m9	0	–	7.8	0.0	–	4.9
B*2705 pGR A	**0.0**	–	8.3	**4.7**	–	6.2
B*2705 pGR B	**0.0**	–	8.2	**6.6**	–	5.9
B*2705 gag	10.5	0	11.0	0.0	–	4.7
B*2705 pEBNA-3C	**18.6**	0	7.7	**0.0**	–	5.7
B*2705 flu	**11.9**	0	8.1	**0.0**	–	5.4
B*2709 S10R	2.3	–	8.6	0.0	–	4.9
B*2705 no peptide	10.2	0	7.6	3.3	–	5.0
B*2705 no peptide, β2m	8.4	0	7.6	3.0	–	5.0
B*2709 no peptide	8.7	0	7.2	2.0	–	4.9
B*2709 no peptide, β2m	8.4	0	7.2	3.4	–	4.9

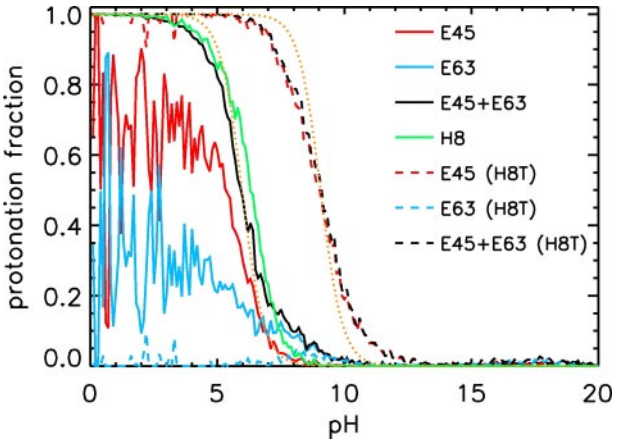

FIGURE 6. **Protonation fraction of selected titratable groups (Glu-45, Glu-63, pHis-8) of HLA-B*2705 with bound pVIPR as a function of the pH value.** The total protonation of Glu-45 and Glu-63 of B*2705 with bound pVIPR (mutated pVIPR-His8Thr) is denoted by a *black line* (*black dashed line*), and the respective Henderson-Hasselbalch fit by a *dotted orange line*.

well as from the crystal structure of the B*2709 complex with the S10R peptide (12, 23). The *collective* pK_a, *i.e.* the pK_a for the coupled protonation of Glu-45 and Glu-63, is 6.0 in the case of pVIPR bound to B*2705 (see Fig. 6, *orange dotted curve* from a least square fit of the Henderson-Hasselbalch equation to the collective titration curve of Glu-45 and Glu-63, *black line*). The protonation state of Glu-45 is not dependent on the presence or absence of the β_2m (Table 4).

Despite a virtually identical environment of Glu-45 in B*2705 presenting the sequence-related pVIPR and pLMP2 peptides, the effective pK_a values for Glu-45 show a drastic shift between these two systems, from 6.0 with pVIPR to 8.8 in the complex with pLMP2. However, the intrinsic pK_a of Glu-45 in the B*2705/pLMP2 complex (pK_a = 8.1, see Table 4), *i.e.* the pK_a value calculated excluding the influence of other titratable groups in their charged state, hardly differs from the value calculated for the B*2705/pVIPR complex (pK_a = 8.0 in both conformations). An analysis of the electrostatic interaction energy of Glu-45 (data not shown) with the most strongly interacting neighboring amino acids (Tyr-7, Tyr-59, Glu-63, Cys-67, and pArg-2) revealed no significant differences for the complexes with pLMP2 and pVIPR in accordance with the structural similarity of the B*2705/pLMP2 and the B*2705/pVIPR B-pockets (11, 14). In addition to the protonation dependence of Glu-45/Glu-63 on the bound peptide and subtype, pLys-3 of pVIPR was found deprotonated when bound to B*2709 (pK_a = 3.6). Taking the peptide-dependent protonation states into account, the peptide-binding free energies of pLMP2 and pVIPR bound to the B*2705/09 subtypes were calculated as outlined under "Experimental Procedures" (detailed in supplemental Table S1).

The difference in binding free energy $\Delta\Delta G_{\text{pLMP2-pVIPR,calc}}$ between pLMP2 and pVIPR B with a salt bridge between pArg-5 and Asp-116 shows a destabilization of 20 ± 6 kJ mol^{-1} for B*2705/pLMP2 and 2 ± 6 kJ mol^{-1} kJ mol for B*2709/pLMP2 compared with HLA-B27/pVIPR, which is in very good agreement with the destabilization energy differences determined experimentally (Table 3). pVIPR bound to B*2705 in canonical conformation (in short pVIPR A; no salt bridge between pArg-5 and Asp-116) resulted in drastically decreased peptide binding strength with respect to the noncanonical conformation and also in comparison with B*2705/pLMP2 (Table 3 and supplemental Table S1). Because of the most likely large differences in the change of entropy upon peptide binding to the different subtypes (16), comparisons of the binding free energy between the subtypes and to other peptides are omitted.

To investigate the influence of the different protonation states of Glu-45 in the B-pocket on the unexpected destabilization of the of the HLA-B27-pLMP2 complexes as revealed by the experiments (Table 3) and the free binding energy calculations (Table 3 and supplemental Table S1), we analyzed the interaction energy (electrostatic and van der Waals energies) between the main anchor residue pArg-2 and the B*2705/09 molecules (HC and β_2m) (supplemental Table S2). The different protonation states of Glu-45/Glu-63 for pLMP2 and pVIPR bound to B*2705 cause a tighter binding of pArg-2 in case of the latter peptide by 24 kJ/mol, similar to the difference in binding free energy between these two complexes (Table 3). For B*2709, however, the increased binding free energy for pVIPR cannot be explained by a tighter binding of the N terminal anchor residue pArg-2. In contrast, pArg-2 is less tightly bound in case of pVIPR (≈10 kJ/mol). The increased affinity of pVIPR to B*2709 as compared with pLMP2 can instead be explained by the deprotonation of pLys-3 upon binding.

In the case of the peptides gag and m9, which both possess a basic Lys residue at pΩ, we additionally analyzed the interaction energy of pLysΩ with the respective subtype. Similar values were found for B*2705/m9 and B2705/gag complexes (supplemental Table S2), both of which contain an additional salt bridge between Asp-116 and pLysΩ. For B*2709/m9, however, the inter-

TABLE 5

Change in free energy of thermal peptide stability for the peptides pLMP2 and pVIPR and their p8 mutants in comparison with each other when bound to the B*2705 subtype

The HLA complexes were compared at pH 7.5. The transition temperatures for peptide unbinding are given in Table 2. The mean values for ΔT_m and ΔS^0 were obtained from the respective data with the fluorescent label attached to pC6. The S.E. is given. For the computed differences in the binding free energy $\Delta\Delta G_{\text{P1-P2,calc}}$ and the interaction energy between pArg-2 and the B*2705 subtype $\Delta E_{\text{pArg-2,calc}}$ see also Tables 3 and 4 and supplemental Table S2. Negative (positive) energy differences denote a destabilization (stabilization) of HLA-B27/P1 complex compared with the respective HLA-B27/P2 complex.

Peptide P1	Peptide P2	$\Delta T_{\text{P1-P2}}$	ΔS^0_{P1}	$\Delta\Delta G_{\text{P1-P2}}$	$\Delta\Delta G_{\text{P1-P2,calc}}$	$\Delta E_{\text{pArg-2,calc}}$
		K	*J mol*$^{-1}$ *K*$^{-1}$	*kJ mol*$^{-1}$	*kJ mol*$^{-1}$	*kJ mol*$^{-1}$
pLMP2 T8H	pLMP2	−2.6 ± 1.0	899 ± 50	−2.3 ± 1.0	−2.9 ± 6.0	+22 ± 6
pVIPR H8T	pVIPR	−4.4 ± 2.9	1524 ± 63	−6.7 ± 4.7	−16.8 ± 6.0	−18 ± 6

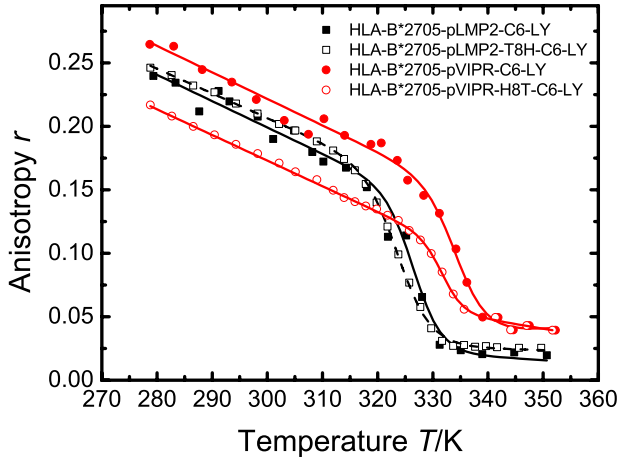

FIGURE 7. **Steady state fluorescence anisotropy of HLA-B*2705/pLMP2-C6-LY (*filled squares*), HLA-B*2705/pLMP2-T8H-C6-LY (*open squares*), B*2705/pVIPR-C6-LY (*filled circles*), and HLA-B*2705/pVIPR-H8T-C6-LY (*open circles*) as a function of temperature.** For B*2705 complexed with pLMP2-C6-LY and pVIPR-C6-LY, each data point represents the mean of five measurements. For B*2705 complexed with pLMP2-T8H-C6-LY and pVIPR-H8T-C6-LY, the temperature-dependent anisotropy curves are an average from two independent measurements. Conditions as in Fig. 3.

action energy of pLysΩ is destabilized by ~30 kJ/mol with respect to the B*2705/m9 complex (supplemental Table S2).

Long Range Effect of Distal Peptide Residues on the Protonation State of Glu-45/63—Surprisingly, the lowering of the Glu-45 pK_a value of B*2705 complexed with pVIPR (pK_a = 6.0) as compared with pLMP2 (pK_a = 8.8) can be attributed to the presence of the distal histidine in position 8 of pVIPR. This was shown by additional pK_a calculations with the histidine in position 8 of pVIPR exchanged with a threonine (as in p8 of pLMP2) (H8T, see Fig. 6 and Table 4). The pVIPR-H8T mutant shows a drastic increase of the collective pK_a value for Glu-45/Glu-63 with respect to B*2705/pVIPR (9.0 instead of 6.4 in the B*2705/pVIPR B complex). Thus, Glu-45 is protonated at physiological pH for B*2705/pVIPR-H8T as well as for B*2705/pLMP2. This result is corroborated by the calculated decrease in interaction energy $\Delta E_{\text{pArg-2}} = -18$ kJ mol^{-1} when comparing B*2705/pVIPR-H8T and B*2705/pVIPR (Table 5) as well as by the decrease in the peptide dissociation temperature of B*2705/pVIPR-H8T compared with B*2705/pVIPR (Fig. 7 and Tables 2 and 5). The free energy differences determined from the experiment $\Delta\Delta G_{\text{pVIPRH8T-pVIPR}}$ (stabilization/destabilization energy) are again in good agreement with the computed free energies of peptide binding $\Delta\Delta G_{\text{pVIPRH8T-pVIPR,calc}}$ (Table 5).

As a crosscheck, a pK_a calculation was performed on the B*2705 subtype complexed with a modified pLMP2 exhibiting pHis-8 in a similar side chain conformation as observed for pHis-8 in pVIPR (see "Experimental Procedures"). As expected, the collective pK_a is decreased (6.1 instead of 8.8) by this mutation similar to B*2705/pVIPR B (6.4), and an increase in interaction energy $\Delta E_{\text{pArg-2}}$ of 22 kJ mol^{-1} (stabilization) was calculated when comparing B*2705/pLMP2-T8H and B*2705/pLMP2 (Table 5). In contrast, the B*2705/pLMP2-T8H complex is destabilized as compared with B*2705/pLMP2, in agreement with the experimentally determined decrease in the peptide dissociation temperature and the negative value (destabilization) of $\Delta\Delta G_{\text{pLMP2T8H-pLMP2}}$ (Fig. 7 and Tables 2 and 5).

As it was found in the literature (23) that an Glu-8/Thr variant of the pEBNA-3C peptide was recognized in the context of B*2705 by KIR3DL1, whereas the natural peptide was not, we performed pK_a calculations on the mutated pEBNA-3C peptide. In contrast to our observations with the pLMP2 and pVIPR peptides, we obtained in the case of the p8 variant of the pEBNA-3C peptide no significant differences with regard to the protonation state of Glu-45 and Glu-63 (data not shown). This result is consistent with the interpretation of Stewart-Jones *et al.* (23) that the direct electrostatic interaction of pGlu-8 with KIR3DL1 is likely to be the cause for the inhibition of KIR3DL1 binding.

Summarizing our results, we found a mutual interaction of peptide and HLA molecule resulting in a peptide- and subtype-dependent protonation pattern of key residues involved in stabilization of the primary peptide anchor pArg-2 (Glu-45/Glu-63, and in case of pVIPR, also of pLys-3). Specifically, our findings show that even a distal, partially solvent-exposed peptide residue (p8) near pΩ at the peptide C terminus may be crucial for binding of the primary peptide anchor in the B-pocket of HLA-B27 molecules.

DISCUSSION

Peptide Stabilizing Effects—As peptide binding is probably central for an understanding of the pathogenic role of HLA-B27 in AS (2, 3), methods allowing the investigation of the molecular interactions governing stable peptide accommodation are mandatory. Peptide affinity studies and high resolution crystal structures of HLA-B27 in complex with individual peptides already shed light on some fundamental rules governing HLA-B27-mediated antigen presentation (10–15, 17, 23, 24, 43). In this study, we have quantified, using experimental as well as theoretical biophysical methods, the effect of the F-pocket residue 116 on the stability of various viral and self-peptides complexed with two HLA-B27 subtypes that are distinguished only by an Asp-116/His exchange. The connection of residue 116 polymorphism to the pathogenesis of other disease states than

AS, like the rate of progression to AIDS in human immunodeficiency virus-positive patients (44) or the outcome of bone marrow transplants between unrelated individuals (45), emphasizes the importance of our study.

Differences between the stabilization/destabilization energies of B*2705 and B*2709 complexes were determined by peptide unbinding studies combined with binding free energy calculations. The latter were based on extensive pK_a calculations for all titratable amino acid residues in the complexes. The resulting interaction energies between the primary peptide anchor pArg-2 and residues belonging to the peptide binding groove were quantified. Depending on the peptide, binding may be stabilized in B*2705 in comparison with B*2709 by an additional salt bridge between Asp-116 and the bound peptide. Although a large stabilization was determined for a pΩ basic residue (pLys-9 in m9 (GRFAAAIAK) and pLys-10 in gag (KRWIILGLNK)), the stabilization energy was about 3–4 times smaller when the salt bridge was formed with pArg-5 (for both pLMP2 RRRWRRLTV) and pVIPR (RRKWRRWHL).

In the light of an understanding of the correlation of B*2705 with the long term nonprogression in chronic HIV infection, this subtype seems to be especially suited for stable accommodation of the gag peptide due to the stabilizing interaction of pLysΩ with Asp-116 in contrast to other subtypes lacking this residue. In the case of B*2709 it is to be expected that HIV-positive individuals might not show a comparable resistance to disease progression, as the interaction with the gag peptide in this subtype is much weaker than in the case of B*2705 (Table 2). However, the very small number of individuals that are both B*2709 and HIV- positive as well as the geographically restricted occurrence of B*2709 (3, 7) will probably preclude a detailed investigation of this problem.

Regarding the observed dual conformation of the self-peptide pVIPR in complex with the subtype B*2705 (11), our results provide strong evidence for the existence of the noncanonical conformation also under physiological conditions. It is noteworthy in this context that recent measurements by infrared spectroscopy suggest an increased flexibility of the B*2705 binding groove compared with B*2709 when complexed with pVIPR (46). Thus higher peptide binding strength as shown here for pVIPR binding to B*2705 can correlate with increased binding groove flexibility.

Destabilization of the Network Anchoring pArg-2—Despite the similar sequences of the viral pLMP2 peptide (RRRWRRLTV) and the self-peptide pVIPR (RRKWRRWHL) as well as similar structural features in the binding groove, including the opportunity to form a noncanonical conformation of the peptide in case of B*2705, a decreased transition temperature for peptide unbinding was found for pLMP2 as compared with pVIPR. For B*2705, our pK_a analyses suggest a tighter binding of the main anchor pArg-2 of pVIPR with respect to pLMP2 as the main reason for this observation: for pVIPR both glutamic acids (45 and 63) that contribute to shaping the B-pocket are deprotonated, although they share one proton for bound pLMP2. The protonation of one glutamic acid results in a drastic decrease in the interaction energy between pArg-2 and the B*2705 binding groove and leads to a less tightly bound pLMP2 peptide as compared with pVIPR. For B*2709, a stabilization of pVIPR with respect to pLMP2 is achieved by a deprotonation of pLys-3 of pVIPR, whereas the environment of the anchor in the second position is unchanged.

The exchange of residue at peptide position 8 between pLMP2 and pVIPR in B*2705 leads to deprotonation or reprotonation of Glu-45/63, suggesting that an intrinsically high pK_a of this pair of residues can be lowered by changing an amino acid residue even at a distant peptide position. In the case of pThr-8 in pLMP2 the distance between the tip of the hydroxyl group of pThr-8 and Glu-45 of the HC is ~22 Å (compare Fig. 1). At this distance, direct Coulomb interactions between the sites are too small to cause the calculated pK_a shift of almost 3 units, thus suggesting an allosteric interaction probably caused by a "cascade effect" through peptide and binding groove leading to the pK_a shift of Glu-45 in the B-pocket. This suggestion is supported by the corresponding change in computed binding free energy, which correlates well with the magnitude of peptide destabilization determined experimentally, expressed as the difference in free energy change $\Delta\Delta G$ upon exchanging pVIPR with pLMP2 in both HLA-B27 subtypes (Table 3). Based on crystallographic analyses of distances between the carboxyl groups alone, a shared proton between Glu-45 and Glu-63 had been suggested before for B*2705 complexes with bound m9, gag, pEBNA-3C, and flu peptides (12, 23) as well as for B*2709 complexed with S10R (12). In contrast, our pK_a analysis revealed low pK_a values for B*2709/S10R and also for B*2709/m9, *i.e.* deprotonated Glu-45 and Glu-63 (error in pK_a estimated to ±1 unit). Despite the expected destabilization of the network anchoring pArg-2 in B*2705/gag through the protonation of Glu-45/63 (Tables 4 and supplemental Table S2), stable peptide accommodation was observed in the experiment (Table 2). The high thermal stability of the B*2705/gag complex is most probably mediated through the additional salt bridge between Asp-116 and pLysΩ, as supported by the computed large interaction energies of pLysΩ with B*2705 (supplemental Table S2). A similar value for the interaction energy of pLysΩ was found for B*2705/m9 (supplemental Table S2). For m9, the interaction energy between pLysΩ and B*2709, however, which lacks Asp-116, is destabilized by ~30 kJ/mol with respect to B*2705 (supplemental Table S2). The theoretical value agrees very well with the experimental finding that for both gag and m9 the interactions of the peptide with the B*2709 are destabilized (Table 2).

Taken together, our combined experimental and theoretical analyses show how the sequence of a bound peptide can influence the protonation states of key residues involved in peptide stabilization. The measured increased binding affinity of the self- peptide pVIPR with respect to the sequence-related pLMP2 peptide of viral origin is because of the deprotonation of HC key residues or peptide residues, Glu-45/Glu-63 in case of B*2705 and pLys-3 in case of B*2709. The peptide- and subtype-dependent protonation pattern of buried key residues involved in stabilization of the primary anchor residue pArg2 were shown to be affected by allosteric effects on electrostatic interactions. The former may have their origin at distal peptide positions. Thus, in addition to peptides with an exchange of pArg-2 also a proper exchange of distal (p8) amino acids (such as pHis-8-Thr between pVIPR and pLMP2 described in this study) may

result in less stable peptide presentation or even failure to present peptides by HLA-B27 antigens. This effect on peptide presentation might have consequences for immune escape mechanisms like those that occur in the context of HIV infections. For the case at hand, Brooks *et al*. (4) have presented evidence that the pLMP2 peptide is less immunogenic when presented by B*2705 than by several other subtypes (B*2709 was not investigated). The unusually high intrinsic pK_a of Glu-45/63 leading to protonation and therefore decreased binding strength for pLMP2 as described above could explain this diminished immunogenicity.

Implications for HLA-B27 Biology and Immune Responses in General—The finding of allele-dependent binding strengths of pArg-2 to the B-pocket is of relevance in the context of theories that seek to explain the still puzzling role of HLA-B27 in AS pathogenesis (2, 3). If the HLA-B27 molecule itself, and not an HLA-B27-linked allele of another locus (47), is primarily responsible for the development of AS, then the B-pocket of HLA-B27 molecules, which is nearly unique among HLA class I molecules (48), must also be scrutinized. It is not only ideally shaped to accommodate a peptide pArg-2 residue (43), but it has also been implicated in the slow folding of the B*2705 subtype (48), which in turn is linked to the increased misfolding within the endoplasmic reticulum that is observed for this subtype (49). The "HLA-B27 misfolding hypothesis" envisages misfolding as the primary event that sets the train leading to the pathological symptoms that characterize AS in motion (19). It has been argued that the differential association of B*2705 and B*2709 cannot be explained by the misfolding hypothesis, because these two subtypes have identical B-pockets and the Asp-116/His exchange has occurred far from the site of primary peptide anchorage (10). However, because of electrostatic interactions, as shown in this study, pArg-2 inside the B-pocket is destabilized when exchanging pVIPR with pLMP2 for B*2705, whereas it is stabilized for B*2709, thus necessitating a revision of this argument. The HLA-B27 subtype-dependent preference for a particular peptide residue (24), possibly far from pArg-2, could influence the stabilization of certain peptides within the binding groove. This might have an impact on the assembly of pMHC within the endoplasmic reticulum as envisaged by Colbert (19). According to another hypothesis (50), HC dimers have been implicated in AS pathogenesis and the production of peptide-devoid HC dimers might be influenced by the presence of peptide or HC residues that indirectly weaken the binding of pArg-2 to the B-pocket.

Apart from shedding new light on problems that are specific to HLA-B27 molecules and their possible involvement in AS pathogenesis, our results are probably also important in the context of cellular immune responses whose strength appears to be directly correlated with the peptide binding affinity to an MHC molecule (51–53). This notion has important implications for the design of peptide vaccines (53), although the experiments are currently restricted to the HLA-A2 allele and a gp100 membrane glycoprotein-derived self-peptide (gp100) as well as a mutated gp100 peptide (T2M) with a Thr/Met exchange at peptide position 2. Functional, structural, and thermodynamic studies have revealed that the elevated T cell response against T2M as compared with gp100 is because of the enhanced stability of HLA-A2-T2M complexes (52, 53). In particular, thermodynamic analyses have proved crucial to understanding the basis of enhanced or diminished immunogenicity of individual peptides in a given allotype.

Although it is currently unclear to what extent the findings with the gp100/T2M system and the conclusions from our results can be generalized, there is agreement that the time span between the initial exposure of a pMHC on the surface of antigen-presenting cells and its eventual recognition by a cytotoxic T cell affect the induction of immune responses (54). As suggested previously (53), the precise knowledge of forces that influence the interactions of a peptide within an MHC peptide binding groove will be indispensable in engineering peptides such that their longevity within the binding groove is improved. Our data demonstrate that a peptide-dependent protonation of B-pocket key residues and a thus altered peptide anchoring must not be neglected in the context of *in silico* vaccine design (for review see Ref. 55). Besides the anchor-fixing approach, a consideration of the effect of distal, even solvent-exposed, peptide residues on the binding properties of the primary anchor appears mandatory.

Acknowledgments—We thank Dr. B. Uchanska-Ziegler (Institut für Immungenetik) for support with the preparation of the HLA-B27/peptide complexes and helpful comments as well as A. Zank and O. Karge for technical assistance.

REFERENCES

1. Allen, R., Bowness, P., and McMichael, A. (1999) *Immunogenetics* **50,** 220–227
2. Kim, T.-H., Uhm, W.-S., and Inman, R. (2005) *Curr. Opin. Rheumatol.* **17,** 400–405
3. Lopez de Castro, J. A. (2007) *Immunol. Lett.* **108,** 27–33
4. Brooks, J., Murray, R., Thomas, W., Kurilla, M., and Rickinson, A. (1993) *J. Exp. Med.* **178,** 879–887
5. Bowness, P., Moss, P., Rowland-Jones, S., Bell, J., and McMichael, A. (1993) *Eur. J. Immunol.* **23,** 1417–1421
6. Wilson, J., Ogg, G., Allen, R., Davis, C., Shaunak, S., Downie, J., Dyer, W., Workman, C., Sullivan, J., McMichael, A., and Rowland-Jones, S. (2000) *AIDS* **14,** 225–233
7. Khan, M. A., Mathieu, A., Sorrentino, R., and Akkoc, N. (2007) *Autoimmun. Rev.* **6,** 183–189
8. D'Amato, M., Fiorillo, M., Carcassi, C., Mathieu, A., Zuccarelli, A., Bitti, P., Tosi, R., and Sorrentino, R. (1995) *Eur. J. Immunol.* **25,** 3199–3201
9. Fiorillo, M., Maragno, M., Butler, R., Dupuis, M., and Sorrentino, R. (2000) *J. Clin. Investig.* **106,** 47–53
10. Hülsmeyer, M., Hillig, R., Volz, A., Rühl, M., Schröder, W., Saenger, W., Ziegler, A., and Uchanska-Ziegler, B. (2002) *J. Biol. Chem.* **277,** 47844–47853
11. Hülsmeyer, M., Fiorillo, M., Bettosini, F., Sorrentino, R., Saenger, W., Ziegler, A., and Uchanska-Ziegler, B. (2004) *J. Exp. Med.* **199,** 271–281
12. Hillig, R., Hülsmeyer, M., Saenger, W., Welfle, K., Misselwitz, R., Welfle, H., Kozerski, C., Volz, A., Uchanska-Ziegler, B., and Ziegler, A. (2004) *J. Biol. Chem.* **279,** 652–663
13. Hülsmeyer, M., Welfle, K., Pöhlmann, T., Misselwitz, R., Alexiev, U., Welfle, H., Saenger, W., Uchanska-Ziegler, B., and Ziegler, A. (2005) *J. Mol. Biol.* **346,** 1367–1379
14. Fiorillo, M., Rückert, C., Hülsmeyer, M., Sorrentino, R., Saenger, W., Ziegler, A., and Uchanska-Ziegler, B. (2005) *J. Biol. Chem.* **280,** 2962–2971
15. Rückert, C., Fiorillo, M., Loll, B., Moretti, R., Biesiadka, J., Saenger, W., Ziegler, A., Sorrentino, R., and Uchanska-Ziegler, B. (2006) *J. Biol. Chem.* **281,** 2306–2316

16. Pöhlmann, T., Böckmann, R., Grubmüller, H., Uchanska-Ziegler, B., Ziegler, A., and Alexiev, U. (2004) *J. Biol. Chem.* **279,** 28197–28201
17. Uchanska-Ziegler, B., Alexiev, U., Hillig, R., Hülsmeyer, M., Pöhlmann, T., Saenger, W., Volz, A., and Ziegler, A. (2006) in *Immunobiology of the Human MHC: Proceedings of the 13th International Histocompatibility Workshop and Congress* (Hansen, J. A., ed) Vol. 1, pp. 138–147, IHWG Press, Seattle
18. Winkler, K., Winter, A., Rückert, C., Uchanska-Ziegler, B., and Alexiev, U. (2007) *Biophys. J.* **93,** 2743–2755
19. Colbert, R. (2000) *Mol. Med. Today* **6,** 224–230
20. Edwards, J., Bowness, P., and Archer, J. (2000) *Immunol. Today* **21,** 256–260
21. Uchanska-Ziegler, B., and Ziegler, A. (2003) *Trends Immunol.* **24,** 73–76
22. Goulder, P., Phillips, R., Colbert, R., McAdam, S., Ogg, G., Nowak, M., Giangrande, P., Luzzi, G., Morgana, B., Edwards, A., McMichael, A., and Rowland-Jones, S. (1997) *Nat. Med.* **3,** 212–217
23. Stewart-Jones, G., di Gleria, K., Kollnberger, S., McMichael, A., Jones, E., and Bowness, P. (2005) *Eur. J. Immunol.* **35,** 341–351
24. López de Castro, J., Alvarez, I., Marcilla, M., Paradela, A., Ramos, M., Sesma, L., and Vázquez, M. (2004) *Tissue Antigens* **63,** 424–445
25. Ramos, M., Paradela, A., Vázquez, M., Marina, A., Vázquez, J., and López de Castro, J. (2002) *J. Biol. Chem.* **277,** 28749–28756
26. Garboczi, D., Hung, D., and Wiley, D. (1992) *Proc. Natl. Acad. Sci. U. S. A.* **89,** 3429–3433
27. Alexiev, U., Rimke, I., and Pöhlmann, T. (2003) *J. Mol. Biol.* **328,** 705–719
28. Becktel, W., and Schellman, J. (1987) *Biopolymers* **26,** 1859–1877
29. Vriend, G. (1990) *J. Mol. Graphics* **8,** 52–56
30. Chinea, G., Padron, G., Hooft, R., Sander, C., and Vriend, G. (1995) *Proteins* **23,** 415–421
31. Nielsen, J. E., and Vriend, G. (2001) *Proteins Struct. Funct. Genet.* **43,** 403–412
32. Nielsen, J., and McCammon, J. (2003) *Protein Sci.* **12,** 313–326
33. Nielsen, J., and McCammon, J. (2003) *Protein Sci.* **12,** 1894–1901
34. Kaminski, G., Friesner, R., Tirado-Rives, J., and Jorgensen, W. (2001) *J. Phys. Chem. B* **105,** 6474–6487
35. Rocchia, W., Alexov, E., and Honig, B. (2001) *J. Phys. Chem. B* **105,** 6507–6514
36. Berendsen, H., van der Spoel, D., and van Drunen, R. (1995) *Computer Phys. Comm.* **91,** 43–56
37. Lindahl, E., Hess, B., and van der Spoel, D. (2001) *J. Mol. Model.* **7,** 306–317
38. van der Spoel, D., Lindahl, E., Hess, B., Groenhof, G., Mark, A., and Berendsen, H. (2005) *J. Comput. Chem.* **26,** 1701–1718
39. Sitkoff, D., Sharp, K. A., and Honig, B. (1994) *J. Phys. Chem.* **98,** 1978–1988
40. Marelius, J., Graffner-Nordberg, M., Hansson, T., Hallberg, A., and Åqvist, J. (1998) *J. Comput. Aided Mol. Des.* **12,** 119–131
41. Binz, A.-K., Rodriguez, R., Biddison, W., and Baker, B. (2003) *Biochemistry* **42,** 4954–4961
42. Dédier, S., Reinelt, S. Rion, S., Folkers, G., and Rognan, D. (2001) *J. Immunol. Methods* **255,** 57–66
43. Madden, D., Gorga, J., Strominger, J., and Wiley, D. (1991) *Nature* **353,** 321–325
44. Gao, X., Nelson, G. W., Karacki, P., Martin, M. P., Phair, J., Kaslow, R., Goedert, J. J., Buchbinder, S., Hoots, K., Vlahov, D., O'Brien, S. J., and Carrington, M. (2001) *N. Engl. J. Med.* **344,** 1668–1675
45. Ferrara, G. B., Bacigalupo, A., Lamparelli, T., Lanino, E., Delfino, L., Morabito, A., Parodi, A. M., Pera, C., Pozzi, S., Sormani, M. P., Bruzzi, P., Bordo, D., Bolognesi, M., Bandini, G., Bontadini, A., Barbanti, M., and Frumento, G. (2001) *Blood* **98,** 3150–3155
46. Fabian, H., Huser, H., Narzi, D., Misselwitz, R., Loll, B., Ziegler, A., Böckmann, R. A., Uchanska-Ziegler, B., and Naumann, D. (2008) *J. Mol. Biol.* **376,** 798–810
47. Cascino, I., Paladini, F., Belfiore, F., Cauli, A., Angelini, C., Fiorillo, M. T., Methieu, A., and Sorrentino, R. (2007) *Arthritis Rheum.* **56,** 2640–2651
48. Mear, J., Schreiber, K., Münz, C., Zhu, X., Stevanovic, S., Rammensee, H.-G., Rowland-Jones, S., and Colbert, R. (1999) *J. Immunol.* **163,** 6665–6670
49. Dangoria, N., DeLay, M., Kingsbury, D., Mear, J., Uchanska-Ziegler, B., Ziegler, A., and Colbert, R. (2002) *J. Biol. Chem.* **277,** 23459–23468
50. Allen, R., O'Callaghan, C., McMichael, A., and Bowness, P. (1999) *J. Immunol.* **162,** 5045–5048
51. Chen, Z., Craiu, A., Shen, L., Kuroda, M., Iroku, U., Watkins, D., Voss, G., and Letvin, N. (2000) *J. Immunol.* **164,** 6474–6479
52. Yu, Z., Theoret, M., Touloukian, C., Surman, D., Garman, S., Feigenbaum, L., Baxter, T., Baker, B., and Restifo, N. (2004) *J. Clin. Investig.* **114,** 551–559
53. Borbulevych, O., Baxter, T., Yu, Z., Restifo, N., and Baker, B. (2005) *J. Immunol.* **174,** 4812–4820
54. Bousso, P., and Robey, E. (2003) *Nat. Immunol.* **4,** 579–585
55. DeGroot, A. S., and Berzofsky, J. A. (2004) *Methods* (*San Diego*) **34,** 425–428